RESEARCH ARTICLE

Dual RNA-seq of Nontypeable *Haemophilus influenzae* and Host Cell Transcriptomes Reveals Novel Insights into Host-Pathogen Cross Talk

Buket Baddal,[a]* Alessandro Muzzi,[a] Stefano Censini,[a] Raffaele A. Calogero,[b] Giulia Torricelli,[a] Silvia Guidotti,[a] Anna R. Taddei,[c] Antonello Covacci,[a] Mariagrazia Pizza,[a] Rino Rappuoli,[a] Marco Soriani,[a] Alfredo Pezzicoli[a]

R&D Centre, GSK Vaccines, Siena, Italy[a]; Department of Molecular Biotechnology and Health Sciences, Molecular Biotechnology Center, University of Turin, Turin, Italy[b]; Center for High Instruments, Electron Microscopy Section, University of Tuscia, Viterbo, Italy[c]

* Present address: Buket Baddal, Division of Infectious Diseases, Boston Children's Hospital and Department of Pediatrics, Harvard Medical School, Boston, Massachusetts, USA.

ABSTRACT **The ability to adhere and adapt to the human respiratory tract mucosa plays a pivotal role in the pathogenic lifestyle of nontypeable *Haemophilus influenzae* (NTHi). However, the temporal events associated with a successful colonization have not been fully characterized. In this study, by reconstituting the ciliated human bronchial epithelium *in vitro*, we monitored the global transcriptional changes in NTHi and infected mucosal epithelium simultaneously for up to 72 h by dual RNA sequencing. The initial stage of colonization was characterized by the binding of NTHi to ciliated cells. Temporal profiling of host mRNA signatures revealed significant dysregulation of the target cell cytoskeleton elicited by bacterial infection, with a profound effect on the intermediate filament network and junctional complexes. In response to environmental stimuli of the host epithelium, NTHi downregulated its central metabolism and increased the expression of transporters, indicating a change in the metabolic regime due to the availability of host substrates. Concurrently, the oxidative environment generated by infected cells instigated bacterial expression of stress-induced defense mechanisms, including the transport of exogenous glutathione and activation of the toxin-antitoxin system. The results of this analysis were validated by those of confocal microscopy, Western blotting, Bioplex, and real-time quantitative reverse transcription-PCR (qRT-PCR). Notably, as part of our screening for novel signatures of infection, we identified a global profile of noncoding transcripts that are candidate small RNAs (sRNAs) regulated during human host infection in *Haemophilus* species. Our data, by providing a robust and comprehensive representation of the cross talk between the host and invading pathogen, provides important insights into NTHi pathogenesis and the development of efficacious preventive strategies.**

IMPORTANCE **Simultaneous monitoring of infection-linked transcriptome alterations in an invading pathogen and its target host cells represents a key strategy for identifying regulatory responses that drive pathogenesis. In this study, we report the progressive events of NTHi colonization in a highly differentiated model of ciliated bronchial epithelium. Genome-wide transcriptome maps of NTHi during infection provided mechanistic insights into bacterial adaptive responses to the host niche, with modulation of the central metabolism as an important signature of the evolving milieu. Our data indicate that infected epithelia respond by substantial alteration of the cytoskeletal network and cytokine repertoire, revealing a dynamic cross talk that is responsible for the onset of inflammation. This work significantly enhances our understanding of the means by which NTHi promotes infection on human mucosae and reveals novel strategies exploited by this important pathogen to cause invasive disease.**

Received 19 October 2015 **Accepted** 20 October 2015 **Published** 17 November 2015

Citation Baddal B, Muzzi A, Censini S, Calogero RA, Torricelli G, Guidotti S, Taddei AR, Covacci A, Pizza M, Rappuoli R, Soriani M, Pezzicoli A. 2015. Dual RNA-seq of nontypeable *Haemophilus influenzae* and host cell transcriptomes reveals novel insights into host-pathogen cross talk. mBio 6(6):e01765-15. doi:10.1128/mBio.01765-15.

Editor Steven J. Projan, MedImmune

Address correspondence to Marco Soriani, marco.x.soriani@gsk.com.

This article is a direct contribution from a Fellow of the American Academy of Microbiology.

The Gram-negative bacterium nontypeable *Haemophilus influenzae* (NTHi) commonly resides in the human nasopharynx, from which it can disseminate to local organs to cause a wide spectrum of diseases, including otitis media (OM), chronic obstructive pulmonary disease (COPD), cystic fibrosis, and bronchitis (1). Successful colonization by NTHi depends on its ability to adhere and adapt to the respiratory tract mucosa, which serves as a frontline defense against respiratory pathogens. In opportunistic infections, colonization is followed by either a paracellular route across the epithelial barrier (2, 3) or invasion of nonphagocytic and epithelial cells. Indeed, wild-type NTHi clinical isolates have been demonstrated *in vitro* and *in vivo* to adhere to and invade a number of cell types mainly by macropinocytosis (4–7).

All bacterial pathogens encounter changes in the environmental conditions within different anatomical sites of the host, which makes rapid adaptation a crucial factor for survival. The course of infection triggers a dynamic cascade of events that culminates in alterations in gene expression patterns in both interacting organisms. To this end, transcriptional reprogramming of host cells is considered to be central to host defense (8). Deciphering this

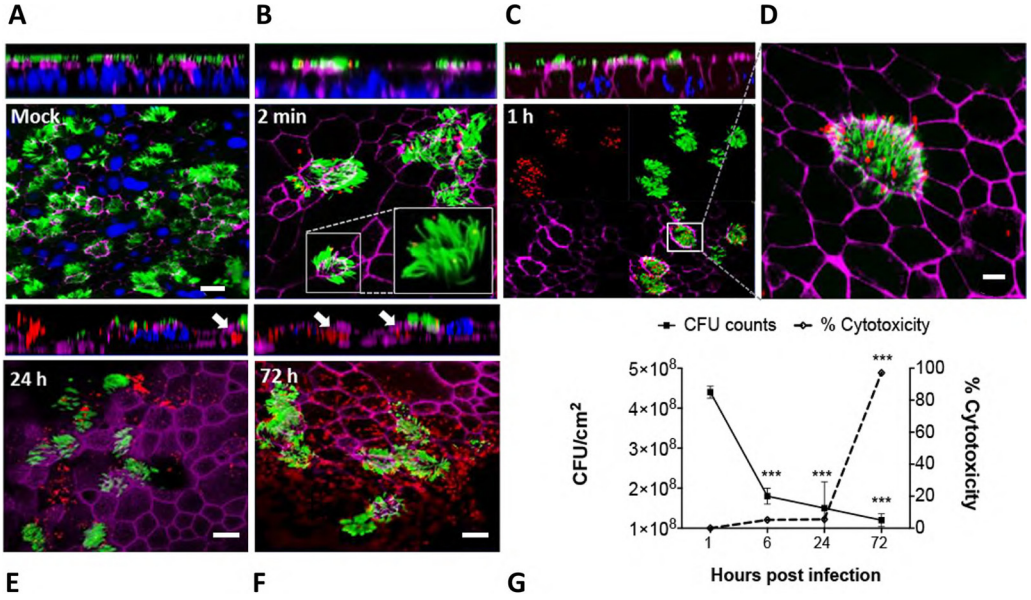

FIG 1 NTHi preferentially targets ciliated cells of primary human bronchial epithelium. (A) Cultured at an air-liquid interface, WD-NHBE cells exhibit a multilayered ciliated epithelium phenotype as observed by confocal microscopy. Bronchial epithelium was stained for phalloidin (magenta) and β-tubulin IV (green); nuclei were counterstained with Hoechst 33342 (blue) (magnification, ×40). (B and C) *En face* and orthogonal sections of NTHi (red)-infected WD-NHBE cells show colocalization of NTHi with ciliated cells as early as 2 min after infection. (D) A single ciliated cell demonstrating NTHi tropism for ciliated cells (magnification, ×100). (E and F) NTHi is internalized into WD-NHBE cells (arrows) and resides within the bronchial epithelium for prolonged periods of time (magnification, ×40). (G) Growth kinetics of cell-associated bacteria and cytotoxicity in host cells over time. Results are expressed as mean values + SEM. One-way ANOVA followed by Bonferroni posttest was used for statistical analysis to compare the results at 6, 24, and 72 h to the results at 1 hpi. ***, $P < 0.001$; no asterisks, not significantly different.

complex interplay is the main aim of host-pathogen interaction studies and serves as the basis of the development of novel therapies and preventative strategies (9). Although several studies have focused on unraveling the molecular mechanisms of adaptation in various respiratory pathogens and/or their hosts (10–13), host-pathogen cross talk during NTHi infections of the human host remains poorly documented.

Recent improvements in tissue engineering techniques, including the development of differentiated primary cell cultures and organotypic 3-dimensional (3-D) cellular models, have significantly increased our understanding of microbial pathogenesis by providing physiologically relevant representations of human upper airway tissue (14–16). Bridging these techniques with the currently available next-generation sequencing technologies is a conceptually promising approach for studying infection-linked transcriptome alterations in such systems. Massively parallel cDNA sequencing (RNA-seq) offers the possibility of comprehensive and simultaneous whole-genome transcriptional profiling of both the host and the invading pathogen and overcomes the existing technical and economical limitations of probe-dependent methods (17).

Taking advantage of the technological advances, here we used an *in vitro* primary ciliated human bronchial epithelium model to monitor the progression of NTHi infection during a time course and analyzed the global gene expression by dual RNA sequencing to simultaneously generate high-resolution transcriptome profiles of NTHi and the human host. To better mimic the *in vivo* situation, we performed prolonged infections of up to 72 h with the continuous bacterial exposure that is likely to happen *in vivo*. This approach identified pathogen-mediated signaling pathways and significant dysregulation of the target cell cytoskeletal network induced by intracellular infection, as well as a specific set of novel small nucleolar RNAs (snoRNAs), micro-RNAs (miRNAs), and small Cajal body-specific RNAs (scaRNAs) that represent novel biomarkers of NTHi-induced infections. The depth of the sequencing applied also enabled the construction of genome-wide, strand-specific transcriptome maps of NTHi in progressive infections, highlighting host adaptation pathways and metabolic signature traits of nasopharyngeal colonization. Taken together, our data represent the first dual-transcriptome analysis of NTHi during dynamic interaction with bronchial epithelium and provide new insights into NTHi pathogenesis.

RESULTS

NTHi preferentially targets ciliated cells of primary bronchial epithelium. To characterize the interactions of NTHi with human bronchial epithelium, primary well-differentiated normal human bronchial epithelial (WD-NHBE) cell cultures were used. Under the defined growth conditions, WD-NHBE cultures form a pseudostratified epithelium with tight junctions (TJs) and adherence junctions (AJs) and contain a high population of ciliated cells (Fig. 1A). The airway epithelium also exhibits transepithelial electrical resistance (TER), mucus secretion (see Fig. S1A to C in the supplemental material), and mucociliary activity, hence representing an environment similar to that of the *in vivo* airway lumen. Differentiated cells were infected from the apical side with NTHi strain Hi176, an isolate from the Finnish otitis media outbreak cohort study. Immunofluorescence microscopy (IFM) analysis showed that cilia are the preferential target for adhesion during the early stage of colonization (Fig. 1B to D). This observation was

further confirmed by scanning and transmission electron microscopy (see Fig. S2A to E in the supplemental material). Microcolonies were evident on the host epithelium at 24 h, with aberrant rearrangements in the actin cytoskeleton. Consistent with previous reports, NTHi colonization was followed by an intracellular stage (Fig. 1E and F). The total cell-associated bacterial load was quantified as 4.4×10^8 CFU/cm^2 at 1 h, while the numbers of viable bacteria recovered from WD-NHBE cells decreased at later time points. Epithelial cell viability was high at 1, 6, and 24 h during the time course but was drastically reduced at 72 h postinfection (hpi), as shown by the results of a lactate dehydrogenase (LDH) assay (Fig. 1G).

Infection triggers host-pathogen transcriptional reprogramming. (i) Simultaneous genome-wide transcriptome analysis during infection. We monitored genome-scale events during the infection by applying dual RNA-seq to infected and mock-infected epithelia at 1, 6, 24, and 72 h postchallenge in three biologically independent experiments per time point. At each time point, between 60 and 180 million total reads per sample were obtained, of which approximately 40 to 80% could be aligned to bacterial and human genomes (see Table S1 in the supplemental material). Reciprocal mapping verified that no reads mapped to the other genome. The reads obtained at different stages of infection were aligned with corresponding genomes to construct transcriptome maps during the temporal progression of infection.

Using *limma*, we identified 1,068 NTHi genes whose expression was either positively or negatively regulated by ≥2-fold (adjusted *P* value of <0.05), with a core set of 151 transcripts being common to all time points of infection (Fig. 2A). The maximum number of differentially expressed (DE) genes was observed at 1 h postchallenge, indicating a rapid organization of the transcriptome already at 1 h in response to the mucosal niche. The genome of Hi176 harbors 1,877 protein-encoding genes, of which the vast majority (87.96%) were represented in our RNA-seq data (see Dataset S1 in the supplemental material), providing comprehensive coverage of the NTHi transcriptome under the conditions used in this study. On the host side, transcriptome analysis of human bronchial epithelium over a 72-h infection time course revealed a total of 1,423 genes to have statistically significant ($P < 0.01$) differential expression (790 genes that were upregulated and 633 that were downregulated) (Fig. 2B and C). Genes were considered to be differentially regulated if they showed, under at least one condition, an average transcript value with a $\log_2$ ratio greater than 1 or less than −1. DE host genes in infected cells compared to their expression in mock-infected cells were identified by calculating reads per kilobase per million (RPKM). For this analysis, the gene expression profiles of cells at 1 h and 6 h after infection were compared with those of mock-infected controls at 1 h, whereas time-matched mock-infected controls were used for comparative analysis of infected cells at 24 and 72 hpi. At 1 h, 110 genes were found to be modulated, with an increase in gene expression dynamics at 6 h for 495 genes, while the numbers showed transient decreases at later time points (see Dataset S2 in the supplemental material).

For the bacterial cells, the projection of differentially regulated transcripts is displayed along the chromosome map of strain Hi176 in Fig. 3A. KEGG pathway analysis revealed that the majority of the DE gene families were involved in protein synthesis, carbohydrate, amino acid, and energy metabolism, and membrane transport (Fig. 3B). On the host side, gene set enrichment analysis using the DAVID (Database for Annotation, Visualization, and Integrated Discovery) functional annotation resource (18) identified significantly enriched functional groups (Benjamini-Hochberg-corrected *P* value [P_{BH}] of <0.05) that were altered by NTHi infection. In order to gain insights into the immediate-early and intermediate-late host responses, we performed joint enrichments of functionally related gene groups, considering all modulated transcripts at 1 h and 6 h together as analysis I and all other transcripts, obtained at 24 h and 72 h, as analysis II (Fig. 4). Additional selected paired analyses were performed with Ingenuity Pathway Analysis (IPA) software in order to map functional networks of relevant genes. The top 5 molecular and cellular functional pathways and top 5 canonical pathways identified by IPA at each time point are listed in Table S2 in the supplemental material.

(ii) Bacteria modulate virulence factor expression during colonization. Several virulence factors that promote NTHi colonization of the nasopharynx and evasion of the host defenses, including a number of adhesins involved in the initial adherence to host epithelium, were significantly differentially regulated across time points. Our data show downregulation of a number of genes encoding proteins associated with the outer membrane already at 1 h. Among them, we found pilin biosynthesis genes *pilA*, *pilD*, and *pilF*; *hap*; *ompP5*, which encodes the NTHi ligand of both epithelial cell intercellular adhesion molecule 1 (ICAM-1) and complement factor H; and *ompE*, which codes for the vitronectin binding protein. In contrast, the gene encoding adhesin Hia, *ompP26*, and the putative surface adhesin-encoding gene *olpA1* were upregulated during infection. Of note, highly conserved toxin-antitoxin (TA) family components were among the genes with the highest transcript levels at 6 h. These include *relBE*, *higBA*, *vapBC1*, *vapBC2*, and *stbDE*, some of which have been implicated in NTHi survival and persistence following stress within the host (19, 20) and have also recently been shown to be involved in niche-specific colonization in *Escherichia coli* (21).

(iii) NTHi infection alters the integrity of host cell junctional complexes. The initial attachment of bacteria to cilia and the apical membrane triggered a dynamic response in host cells, as observed by DAVID I enrichment of several functional groups, including response to hypoxia, regulation of cell cycle and cell death, regulation of cell differentiation, and negative regulation of apoptosis (Fig. 4). Importantly, this analysis also deduced that NTHi exposure profoundly affected epidermis development, as well as the anchoring and adherence junctions of target cells. Within our 6-h data set, the cross-linking small proline-rich protein SPRR1B was upregulated more than 2-fold (Fig. 5A), suggesting a previously unrecognized mechanism of adaptive host bronchial epithelial defense toward respiratory bacterial pathogens. Another group of proteins contributing to epithelial cell integrity highlighted in this analysis was part of the cadherin family. Among these Ca^{2+}-dependent transmembrane cell adhesion molecules (CAMs), which mediate cell-cell interaction, we noted a 2-fold reduction in protocadherin 8 (PCDH8) and an almost 4-fold decrease in cadherin 6 (CDH6). The transcriptome signatures also revealed modulation of cell-to-cell junction proteins, in particular claudin 3 (CLDN3) and claudin 8 (CLDN8), which serve as the sealing components of the TJs forming the paracellular barrier, highlighting the activation of a mechanism of bacterial invasion based on paracytosis. γ-Adducin (ADD3γ), which represents an important constituent of the spectrin-actin network, and the

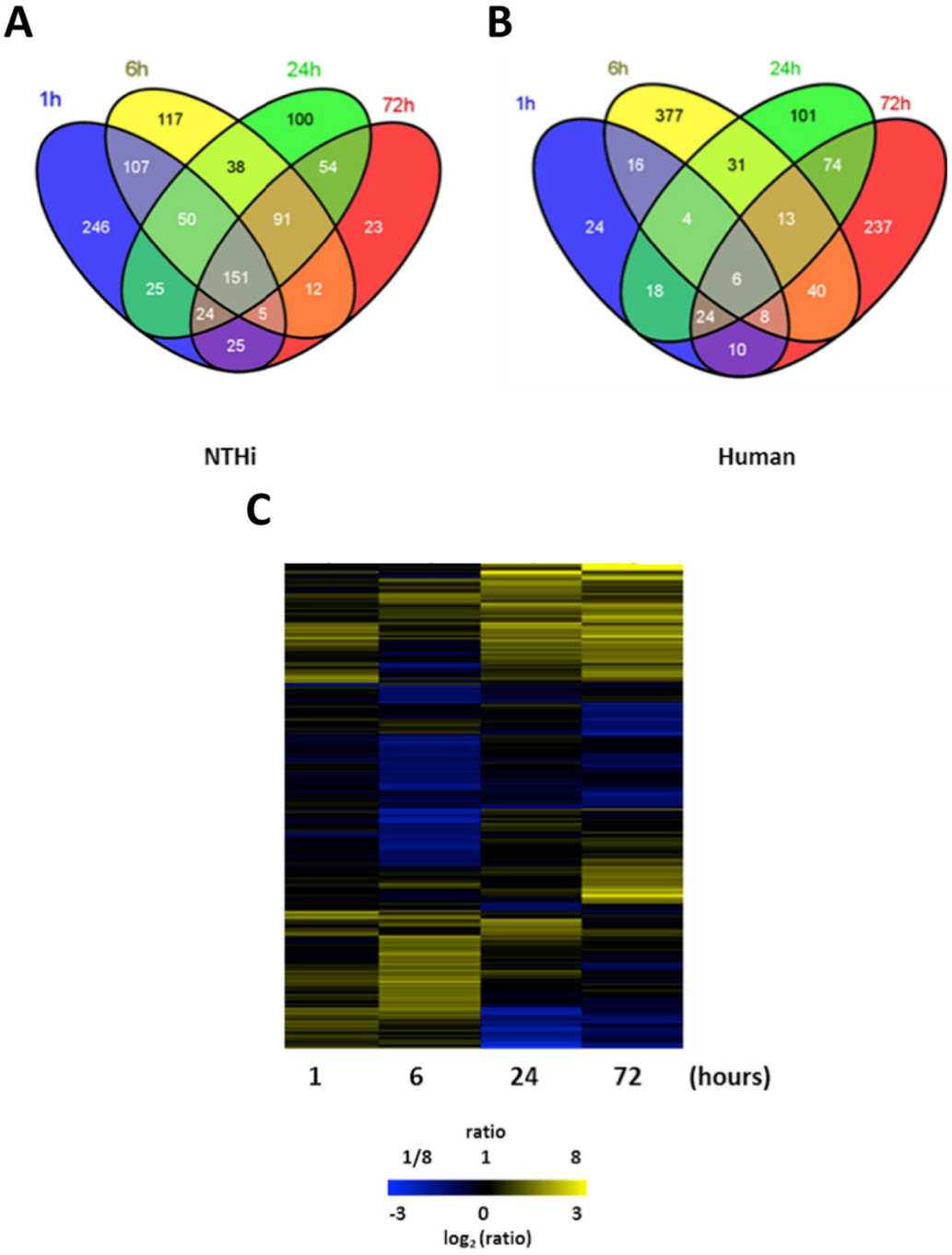

FIG 2 Overview of whole-transcriptome data. (A) Venn diagram showing the number of differentially expressed genes per comparison across time points and the overlap between each set of genes. Data for NTHi transcripts that were commonly differentially regulated ($\log_2$-fold change of ≥ 1, $P < 0.05$) are shown. The total numbers of genes per time point are 633 at 1 h, 571 at 6 h, 533 at 24 h, and 385 at 72 h. (B) Data for human transcripts that were commonly differentially regulated ($\log_2$-fold change of ≥ 1, $P < 0.01$) are shown. The total numbers of genes per time point are 110 at 1 h, 495 at 6 h, 271 at 24 h, and 412 at 72 h. (C) Heat maps of host gene expression during infection time course. The read counts of each cellular mRNA were normalized by the sum of the total reads. Colors from black to yellow indicate upregulated cellular genes; colors from black to blue indicate downregulated cellular genes.

actin-related protein 2/3 complex, subunit 2 (ARPC2), which is implicated in the control of actin polymerization, were within the set of genes downregulated at 6 hpi. The alterations in the mRNA expression levels of CDH6, CLDN3, and ADD3γ correlated closely with a reduction in protein expression following NTHi infection (Fig. 5B).

(iv) NTHi metabolic machinery adapts to host-imposed milieu. The transcriptome signatures showed that, while transport machineries involved in the uptake of nutrients available from host cells were mainly active during infection, overall, the genes encoding the bacterial biosynthesis pathways of carbohydrates, lipids, amino acids, nucleotides, and energy metabolism were

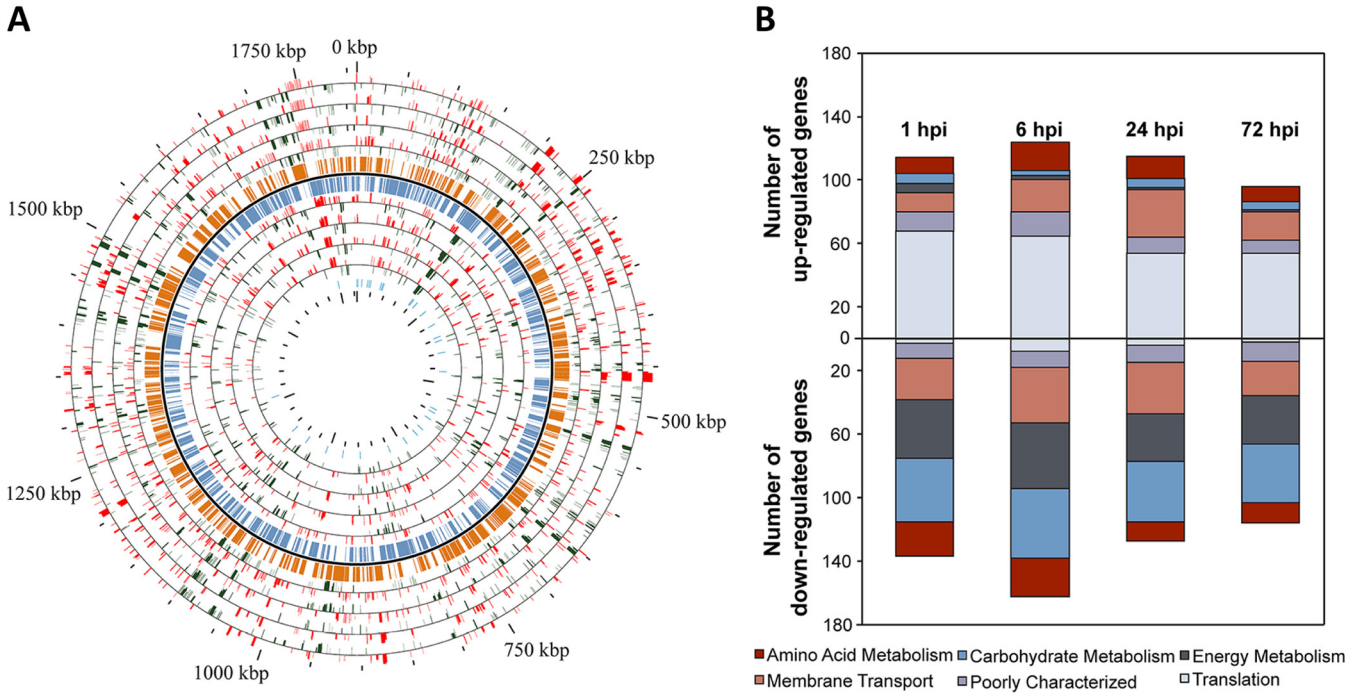

FIG 3 Temporal expression dynamics of NTHi during host infection. (A) Genome-wide NTHi transcriptome map during 72 h of host infection. At various time points, DE genes showing ≥2-fold change ($P < 0.05$) were selected. Transcripts expressed on the reverse strand (internal rings) and forward strand (external rings) are shown. Only sense transcripts are represented. The most internal ring (blue bars) illustrates contig edges. Time points are specular with respect to the chromosome rings: the closest to the chromosome is 1 h, followed by 6 h, 24 h, and 72 h after infection. Red/green color scale represents up- or downregulation of genes. (B) KEGG pathway (subrole) analysis showing the time course of the distribution of genes during metabolic adaptation of NTHi to host bronchial epithelium.

downregulated on a large scale. In particular, the lactate permease gene *lctP*, the arginine regulon *artPIQM*, the tryptophan-specific transport protein *mtr*, the genes encoding the CydD and CydC components of the cysteine/glutathione ATP-binding cassette (ABC) transporter, and the *thiBPQ* operon, which is required for transport of thiamine and thiamine pyrophosphate, with a primary role in central metabolism as an electron carrier and nucleophile (22), were highly expressed. Interestingly, although it was not active during initial contact with host cells at 1 h, we observed specific upregulation of bacterial branched-chain amino acid metabolism. The Shikimate pathway for precursor chorismate production and the consequent tryptophan biosynthesis pathway

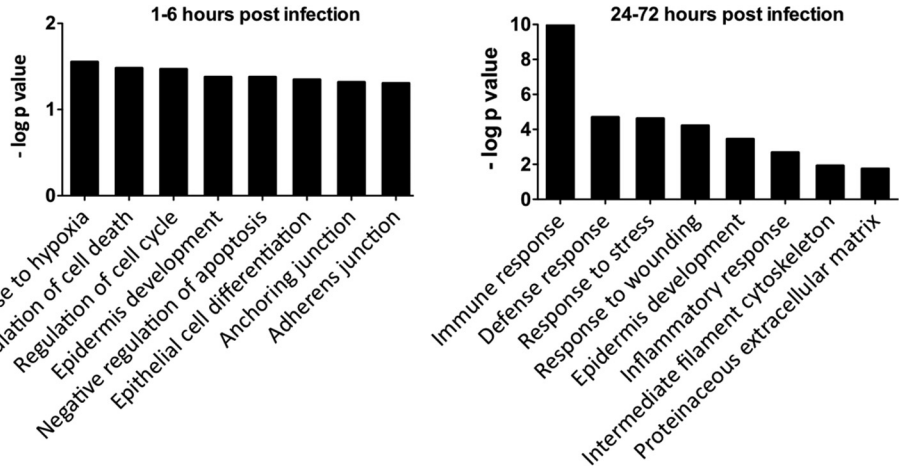

FIG 4 Analysis of host mRNA changes during NTHi infection. Enrichment of functional groups by DAVID is shown, where genes which were differentially expressed in the 1-to-6-h and 24-to-72-h groups were analyzed. Enriched functional groups ($P_{BH} < 0.05$) were identified, and groups representative of the overall enrichment results are shown. Overrepresented categories at 1 to 6 h include response to hypoxia, regulation of cell death, epidermis development, and anchoring and adherens junction; those at 24 to 72 h include immune response, response to stress, epidermis development, inflammatory response, proteinaceous extracellular matrix, and intermediate filament cytoskeleton.

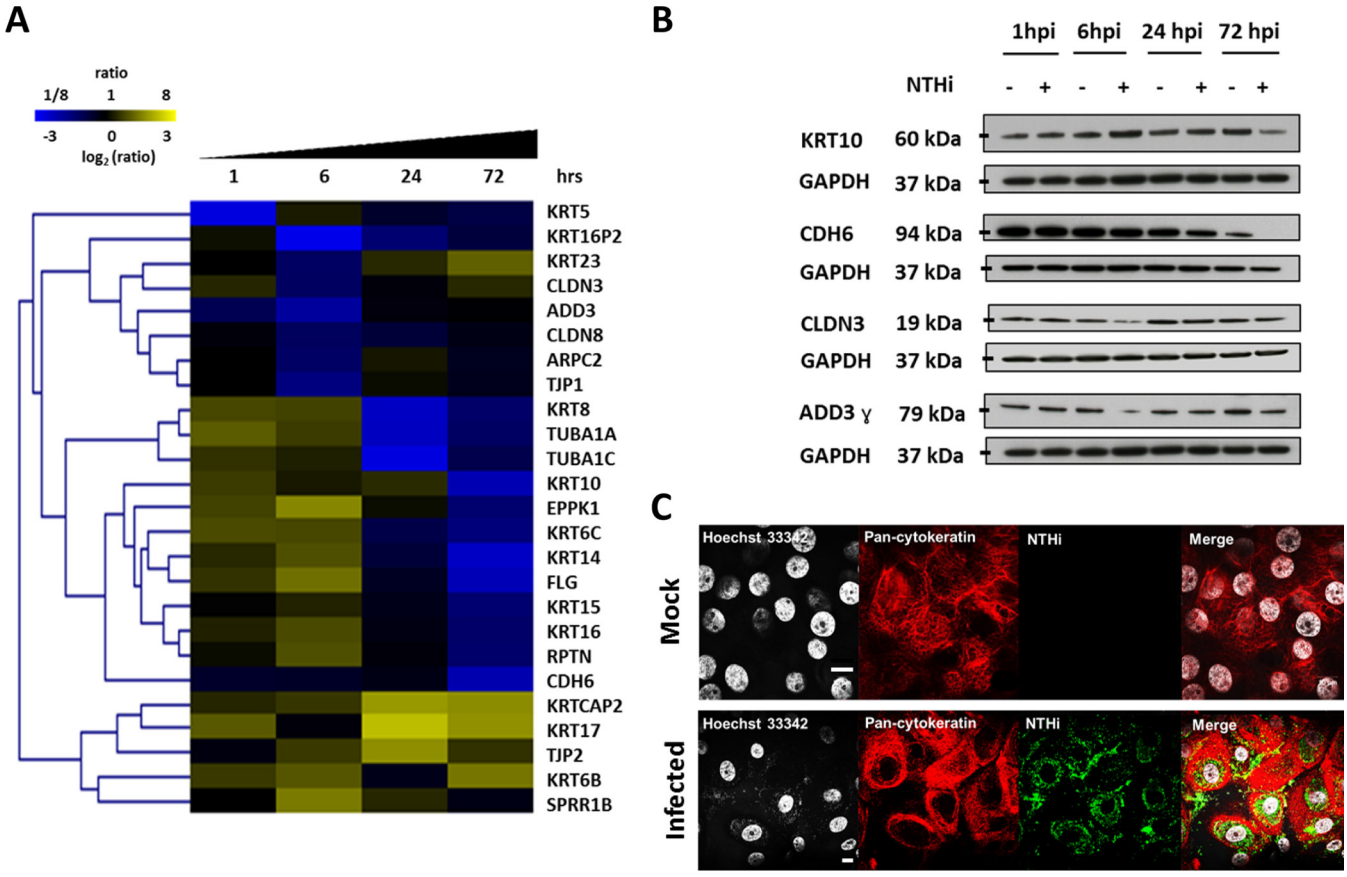

FIG 5 Functional characterization of host transcriptome signatures. (A) Selected heat map analysis of genes identified by gene ontology (GO) term enrichments, in particular, epidermis development, intermediate filament cytoskeleton, and cell-to-cell junction. (B) Protein extracts were analyzed by immunoblotting for suprabasal keratin 10 (KRT10), cadherin 6 (CDH6), claudin 3 (CLD3), and γ-adducin (ADD3γ) expression at 1, 6, 24, and 72 h in mock-infected cells and after NTHi exposure. (C) Immunofluorescence staining of NTHi-infected and uninfected WD-NHBE cells indicates overall reorganization of the keratin intermediate filaments induced by invasive NTHi infection versus the organization of the keratin network in mock-infected epithelia. High-resolution analysis of infected cells at 72 h demonstrates depolymerization of keratin bundles and loss of overall architecture induced by NTHi infection, visualized by pan-keratin antibody staining (magnification, ×40).

were also upregulated. The expression of several aminoacyl tRNA synthetase genes (*pheST*, *lysU*, and *valS*) was induced, whereas the expression of eight enzymes mainly involved in the biosynthesis of the essential amino acid histidine in NTHi, encoded by eight genes (*hisG*, *-D*, *-C*, *-B*, *-H*, *-A*, *-F*, and *-IE*) organized in an operon, was highly downregulated, suggesting the availability of histidine from host cells. An upstream *his* leader element was identified as an intergenic region of high transcriptional activity that may act as an attenuator of the operon (Fig. 6). Iron is an important factor for NTHi survival and persistence in the human host. Consistent with the nature of the organism, our data indicate strong upregulation of the ferric hydroxamate ABC transporter operon *fhuCDBA*, by up to 12-fold, in a time-dependent manner, with the expression particularly increased after 24 h of adaptation, as well as strong upregulation of the *hitABC*-encoded transporter, a highly conserved, siderophore-independent, high-affinity iron acquisition system (23). Another transport system with a high expression profile belongs to the family of polyamines, which are essential for normal cellular growth and multiplication of prokaryotic cells. The *potABCD* operon, with genes coding for spermidine/putrescine uptake and transport, was increasingly activated.

Transcriptome signatures highlight progression of infection. (i) Bacterial stress response elements are activated at late stages of infection. Under the experimental conditions used, we observed an increased number of intracellular bacteria during infection. In this context, NTHi encounters and must adapt to numerous stressors generated endogenously by host cells or copathogens, most notably oxidative stress. Indeed, we found the *dppBCDF* operon, which is involved in glutathione (GSH) transport in *Haemophilus* spp. (24), to be highly upregulated. In addition, transcript changes were observed for stress response genes like *oxyR*, the hydrogen peroxide-inducible gene activator and global regulator of the OxyR regulon, which has been demonstrated to comprise 11 genes in strain 86-028NP (25), with more than 2-fold upregulation at 1 h of host infection. Within the members of this regulon, we found increased expression of *pgdX*, encoding peroxiredoxin/glutathione-dependent peroxidase, as well as *pntA* and *pntB*, which encode the α and β subunits of NAD(P) transhydrogenase. PgdX has recently been reported to be important for NTHi persistence *in vivo* and to promote survival in neutrophil extracellular traps (26). With a role in acid tolerance in the respiratory tract (27), members of the urease gene cluster *ureAB-*

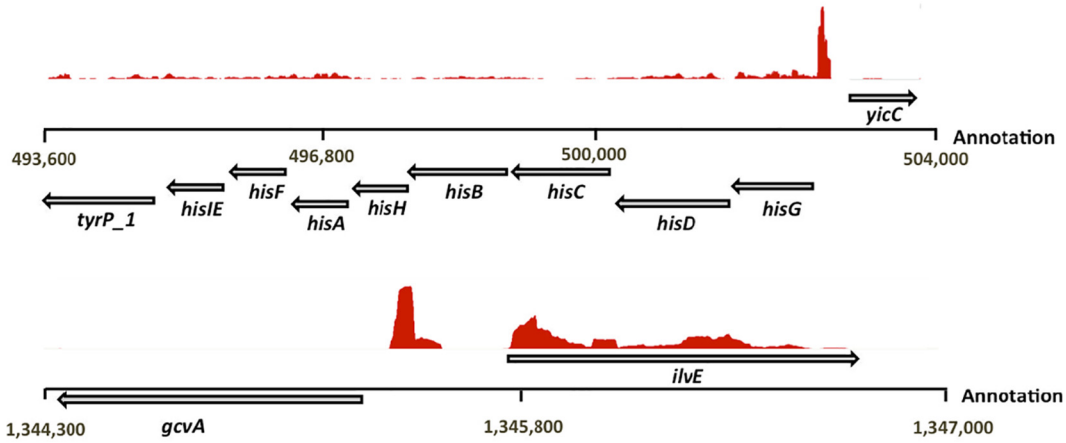

FIG 6 Artemis viewer curation of *his* leader and *gcvB*. *his* leader, an attenuator of the *his* operon, and *gcvB*, encoding a sRNA involved in regulation of amino acid biosynthesis genes, were identified as areas of high transcriptional activity within intergenic regions of the Hi176 genome. Expression data at 1 h of host cell infection are indicated for annotated genes on the minus strand (*his* leader) and on the plus strand (*gcvB*). The read count scale is 0 to 500 for *gcvB* and 0 to 550 for *his* leader.

CEFGH, encoding the urease γ, β, and α subunits and the EFGH accessory proteins, respectively, were found to have elevated transcript levels. In this scenario, host cells which harbor increasing numbers of bacteria activate intracellular pathways like that of lysosome-associated membrane protein 3 (LAMP3), which was induced more than 20-fold. One of the requirements of a successful adaptation of NTHi to the host mucosal surface is the ability to form and reside in a biofilm, as has often been reported for both *in vitro* and *in vivo* experiments. The integration host factor (IHF), belonging to the DNABII family, has a role in the structural stability of the biofilm extracellular matrix (ECM) because of its interaction with extracellular DNA (28). In agreement with this scenario, we observed that the expression of *ihfA* and *ihfB* was upregulated at 6 h and onward during infection of the primary human bronchial epithelium.

(ii) NTHi induces cytoskeletal and ECM rearrangements in host cells. As a consequence of prolonged NTHi infection, significant alterations in the host cell transcriptome were evident, with many of the most highly downregulated genes being associated with cytoskeletal rearrangements (Fig. 5A). IPA (see Table S2 in the supplemental material) further elucidated the enrichment of the cellular assembly and organization module, confirming the formation of cellular protrusions and membrane ruffling (see Fig. S2F), followed by disruption of the cytoskeleton. In particular, epidermis development, intermediate filament (IF) cytoskeleton, and proteinaceous ECM components were within the overrepresented categories in DAVID analysis II. We found a specific cluster of genes with modulated expression, comprised of type I acidic and type II basic-neutral cytokeratins (CK), in particular KRT5, KRT16P2, and KRT23 during the first 6 h, as well as KRT6B, KRT6C, KRT8, KRT10, KRT14, KRT15, and KRT17 at later stages of infection. Filaggrin (FLG), which specifically binds to CK, causing their aggregation into a tightly packed parallel-array network, was also downregulated. The reduction in mRNA expression was confirmed at the protein level, as demonstrated by a reduction in suprabasal KRT10 expression at 72 hpi (Fig. 5B). On the basis of these results, we aimed to further investigate the overall organization of the keratin IFs during intracellular NTHi infection. IMF staining of the keratin network in infected and uninfected epithelia demonstrated substantial reorganization of keratin filaments in infected cells, with complete depolymerization of keratin bundles associated with cell-cell adhesion being evident (Fig. 5C). ECM is a dynamic network controlling the architecture, elasticity, and tensile strength of tissues (29). In our RNA-seq data, many host ECM moieties, including genes encoding fibrillin 2 (FBN2), hemicentin 1 (HMCN1), laminin β3 (LAMB3), collagen type VII (COL7A1), cartilage intermediate layer protein (CILP), and the zinc-dependent matrix metallopeptidases MMP13, ADAMTSL3, ADAMTS15, ADAM9, and ADAM17, were differentially regulated, suggesting a dramatic remodeling of bronchial ECM following NTHi infection. Importantly, upregulation of MMP1 (collagenase I) and MMP9 (gelatinase I) has been proposed to lead to degradation of ECM proteins, allowing further migration of immune cells to the site of infection. Considering the ECM remodeling that takes place during COPD pathophysiology, such as changes in mucosal tissue fiber types and/or fibrosis (30), our results support the physiological relevance of the model used.

(iii) Inflammatory modules are triggered following NTHi infection. Inflammation is a hallmark of both OM and COPD induced by NTHi, which is mainly mediated by inflammatory cytokines and chemokines, such as interleukin 1β (IL-1β), IL-8, and tumor necrosis factor alpha (TNF-α). Notably, IPA (see Table S2 in the supplemental material) indicated strong induction of cell-to-cell signaling, immune cell trafficking, cellular movement, cellular development, and inflammatory response modules within 24 h, with infiltration and chemotaxis of granulocyte functions having the highest activation score. The components of the innate immune response, particularly CXCL5, CXCL10, CXCL11, CCL5, IL-1α, IL-8, and IL-23α, were among the most upregulated genes, highlighting the recruitment of T cells and macrophages to the lungs, a phenomenon associated with airway inflammation during stable and acutely exacerbated COPD (31). To confirm these results, we analyzed the basal secretions of infected WD-NHBE cells for the presence of a panel of 40 chemokines, confirming the marked increase in the secretion of inflammatory response components IL-1β, IL-8, TNF-α, CXCL9, CXCL10, CXCL11, CCL2, and CCL3 elicited by NTHi infection in host bronchial epithelium

TABLE 1 Selected NTHi candidate small noncoding regulatory RNAs with high transcriptional activity during host infection identified by RNA-seq

Transcript	Homologous sRNA family[a]	*E* value	Genome coordinates	Size (nt)	Validation[b]
Hinc1			56,261–56,385	125	−
Hinc2			126,528–126,708	181	−
Hinc3			149,794–149,889	126	−
Hinc4			214,371–214,462	92	−
Hinc5			289,759–289,932	174	−
Hinc6	His leader	2.1E−13	502,489–502,702	214	−
Hinc7			794,881–795,067	187	−
Hinc8			1,026,603–1,026,809	207	−
Hinc9			1,082,498–1,082,758	261	−
Hinc10	tmRNA	4.3E−41	1,154,662–1,154,991	330	−
Hinc11	RNase P	3.8E−35	1,257,046–1,257,364	319	−
Hinc12			1,323,992–1,324,278	287	−
Hinc13	GcvB	1.9E−26	1,345,230–1,345,587	356	−
Hinc14	sSRP	3.5E−14	1,380,444–1,380,550	107	−
Hinc15	HrrF		1,383,458–1,383,597	140	+ (58)
Hinc16			1,563,833–1,564,055	223	−
Hinc17	Glycine	3.9E−15	1,647,278–1,647,664	387	−
Hinc18			1,661,507–1,661,648	142	−

[a] Homology to known sRNA families according to the search against the Rfam database is shown, with the corresponding E value in the next column.
[b] −, not validated; +, previously validated in the indicated study.

(see Fig. S3). No significant changes were detected in the levels of granulocyte-macrophage colony-stimulating factor (GM-CSF), IL-6, and IL-10 in the infected cells (data not shown).

RNA-seq analysis identifies small RNA (sRNA) regulatory elements that are modulated during infection. Deep sequencing of infected bronchial cells also revealed several snoRNA, miRNA, and scaRNA species to be DE during NTHi infection. Notably, we observed a discrete set of 63 host snoRNAs to be differentially regulated that have not previously been reported to be associated with NTHi infection (see Fig. S4 in the supplemental material). These metabolically stable RNAs were categorized into 2 main groups, 33 C/D box type (SNORD) and 30 H/ACA box type (SNORA), which showed a trend of significant upregulation. In addition to this, 10 miRNA precursor signature genes were found to be specifically downregulated within the first 6 h, while the expression of small Cajal body-specific RNA 1 (SCARNA1) and SCARNA11 was enhanced by more than 2-fold following NTHi infection. These data are indicative of novel biomarkers of NTHi-induced diseases.

Reports on posttranscriptional regulation by sRNAs in *Haemophilus* spp. are very limited. As a part of our sequencing screen for novel transcripts, we identified at least 17 novel putative sRNAs in the intergenic regions with high transcriptional activity (Table 1). Six of these are homologous to known sRNA families (RNase P, transfer-messenger RNA [tmRNA], small signal recognition particle [sSRP], glycine, *his* operon leader, and GcvB). Importantly, *gcvB*, encoding a sRNA that is involved in the regulation of multiple amino acid and peptide ABC transporters, was detected upstream from *gcvA* (Fig. 6). The *gcvA* gene codes for the LysR-type transcriptional regulator of the glycine cleavage system and controls transcription of *gcvB* depending on the cellular glycine levels. GcvB has been reported to target and effectively repress the translation of mRNAs that commonly code for periplasmic substrate-binding proteins, such as OppA (repressed in our study), by binding to C/A-rich regions via its conserved G/U-rich elements (32). HrrF, a recently validated Fur-regulated sRNA in *Haemophilus* (33), was also present in our data set.

DISCUSSION

Simultaneous monitoring of the host-pathogen interplay through transcriptome profiling has been a highly challenging aspect of infection biology, mainly due to the inability of array-based techniques to concurrently capture and analyze prokaryotic and eukaryotic transcripts from model systems. In recent years, the consolidation of Illumina-based RNA-seq methodology has allowed simultaneous RNA profiling of a variety of host-pathogen systems, providing new perspectives in our understanding of infection processes (34, 35). In the current report, we describe the first study to generate comprehensive transcriptome profiles of NTHi and its human host in order to capture key features during progressive stages of infection of a highly differentiated primary ciliated human bronchial epithelium. The crucial events occurring during the interplay between NTHi and host cells, highlighted by our transcriptomic analysis and validated by a number of lines of *in vitro* evidence, are summarized in Fig. 7. However, given the enormous genetic, antigenic, and pathogenic diversity among NTHi isolates, the proposed scenario may vary for strains other than the one used in the study.

Notably, we observed that the early contact of NTHi with the bronchial epithelium occurs at the cilium level, which may lead to a decrease in ciliary beat frequency (36). Spondin 2 (SPON2), a pattern recognition receptor (PRR) molecule (37), was the most upregulated protein of the extracellular matrix, indicating an important role for this PRR in NTHi recognition and clearance. As previously reported (38), NTHi is able to modulate the expression of carcinoembryonic antigen (CEA)-related cell adhesion molecule 1 (CEACAM1) in bronchial epithelial cells. In our data set, we observed enhanced expression of CEACAM7, as well as ICAM-1. NTHi recognition further triggers intracellular signaling events that result in rearrangements of the cell cytoskeleton and alteration of junctional complexes, including claudins. Similar observations have been described by Clarke et al. (39), who demonstrated Toll-like receptor (TLR)-dependent downregulation of CLDN7 and CLDN10 by type B *H. influenzae* in the polarized bronchial

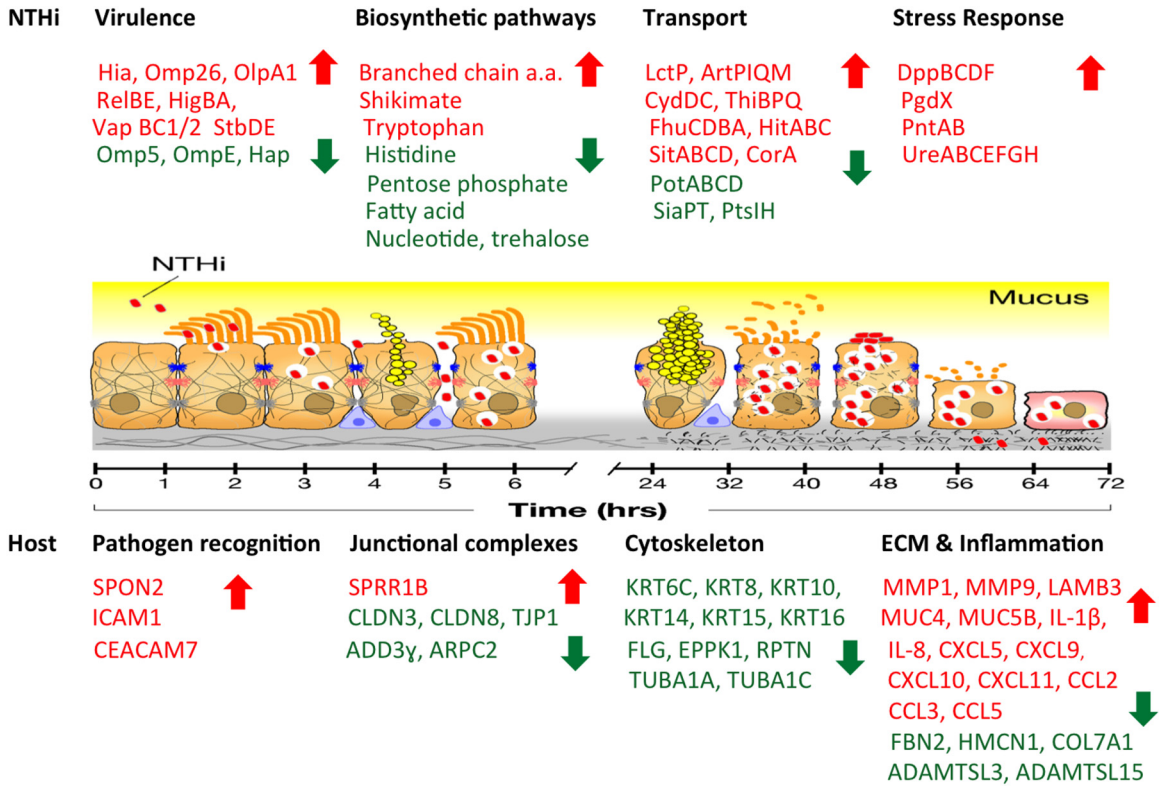

FIG 7 Schematic diagram illustrating the proposed model of pathogenesis of NTHi infection as derived from transcriptome responses and microscopy observations. NTHi binding to ciliated cells triggers a number of events in host cells that lead to large-scale rearrangement of cytostructural integrity and chronic inflammation. Ciliated, mucus-secreting goblet, and basal cells of the respiratory epithelium are represented schematically. The time-dependent modulation of cellular pathways is indicated by the font colors (red, upregulation; green, downregulation). a.a., amino acids.

16HBE14o− cell line, as well as in *in vivo* experiments. The membrane skeletal protein γ-adducin is localized at spectrin-actin junctions; it binds calmodulin and is an *in vivo* substrate for protein kinase C (PKC) and Rho-associated kinases. It regulates the remodeling of AJs in human epithelial cells and has been reported to be redistributed during bacterial infections (40). The downregulation of γ-adducin in our model of the bronchial epithelium gives intriguing insights into a potential role of this protein in the loss of stabilization of epithelial junctions during respiratory infections. From the bacterial perspective, the interaction with the host epithelium initiates a well-defined, time-dependent modulation of key prokaryotic elements that indicates progressive bacterial adaptation. Indeed, at early stages, NTHi not only modulates the expression of adhesins likely to act as the frontline of infection but also activates a large proportion of the genes encoding transport machineries, including those involved in the uptake and utilization of iron/heme, transporters of amino acids, vitamins, metal ions, and sodium, and ATP-binding cassette (ABC)-type transporters. This is representative of an altered bacterial metabolic regime due to the evolving substrate availability. In particular, at late stages of infection when bacteria are observed to be mostly paracellular or internalized, the shift in lifestyle leads to the downregulation of the central metabolism. This includes but is not limited to glycolysis, gluconeogenesis, the pentose phosphate pathway, fatty acid biosynthesis, and nucleotide sugar and trehalose biosynthesis. On the other hand, genes involved in the uptake of lactate and conversion of L- and D-lactate to pyruvate and acetyl-coenzyme A (CoA) are highly upregulated during the entire experiment, suggesting that lactate, which is present in respiratory mucosa, could be a primary carbon and energy source. This finding correlates with recent work demonstrating that lactate is a fundamental carbon source for bacterial pathogens colonizing human mucosal environments (41, 42).

As the infection progresses, NTHi is subjected to increasing chemical and physical stress conditions by host cells. In this context, we found that the *dppBCDF* operon, primed for glutathione transport in *Haemophilus* spp., was highly activated, indicating a crucial need for this important antioxidant reservoir during colonization of host niches. Interaction between keratins and invading pathogens is an emerging concept, and various pathogens have been shown to achieve intracellular persistence through modulation of keratin filaments in terms of expression, rearrangement, induction of dysfunctionality, and cleavage (43, 44). Here, we demonstrate that NTHi leads to substantial dysregulation of the cytokeratin network, leading to instability of the epithelial barrier, as highlighted by overrepresented categories like intermediate filament cytoskeleton and proteinaceous ECM in DAVID analysis II. Loss of cytoskeletal integrity and increased epithelial permeability are usually hallmarks of inflammation. In agreement with this scenario, IPA demonstrated the induction of cell-to-cell signaling, immune cell trafficking, cellular movement, cellular development, and inflammatory response modules within 24 h.

In summary, during progressive infection of the bronchial epithelium, NTHi reprograms its transcriptional machinery to op-

timally benefit from the host milieu and withstand stress conditions it may encounter. In return, infection alters the structure and integrity of the ciliated bronchial epithelium, a condition that is coupled to immune modulators, leading to the onset of disease. Here, we present a valuable data resource that informs the regulation of the majority of NTHi genomic determinants under conditions that mimic the first stages of bacterial infection. However, one limitation of our study is that the dynamics of the events may affect the transcriptome evaluation. Indeed, during each time point, bacteria exist in different cell cycle states and cellular localizations, while eukaryotic cells are exposed to a different number of bacteria, resulting in a mixed population of transcripts that is averaged by the analysis. Nevertheless, the proposed model allows a plausible assessment of gene modulation during NTHi infection of human mucosae. Importantly, we observed that a significant portion of the highly upregulated genes were annotated as having an unknown function or no clear cellular localization of their products. Therefore, our attempt to reproduce a temporal infection model could be taken as a unique opportunity to disclose new factors that may act as important players in NTHi pathogenesis. Using this approach to monitor the expression dynamics of virulence factors in real time represents a novel tool to complement classical screening procedures used for NTHi vaccine discovery, with a potential application to other bacterial pathogens.

MATERIALS AND METHODS

Primary airway epithelial cells. Primary normal human bronchial epithelial (NHBE) cells (isolated from a single healthy donor) were purchased from Clonetics-BioWhittaker (San Diego, CA) and used under the terms and conditions indicated by the provider. The cells were expanded in 75-cm^2 flasks, using bronchial epithelial basal growth medium (BEBM; Lonza) supplemented with the BEGM (bronchial epithelial cell growth medium) BulletKit (catalog no. CC-3170), as recommended by the supplier, at 37°C in 5% CO_2 until ~80% confluence and used between passages 1 and 3. Then, the cells were dissociated using StemPro Accutase cell dissociation reagent (Life Technologies) and were seeded onto semipermeable membrane supports (12-mm diameter, 0.4-μm pore size; Costar) that were previously coated with a solution of collagen type I from rat tail (Gibco) at a concentration of 0.03 mg/ml. The cells were seeded at a density of 10^5 cells per well using bronchial air-liquid interface (B-ALI) medium (Lonza) supplemented with the B-ALI BulletKit (catalog no. 193514). When confluence was reached, the apical medium was removed, and an air-liquid interface was established to trigger differentiation. Cells were maintained at the ALI for at least 28 days prior to use in biological assays, with the basolateral medium being changed every second day, to ensure a differentiated cell population with a mucociliary phenotype. The apical side was rinsed with phosphate-buffered saline (PBS) every week to remove excess mucus production. Cell polarity and TJ barrier function were verified by transepithelial electrical resistance (TER) using an epithelial volt ohmmeter (EVOM^2; World Precision Instruments). Mucus production and cilium development were monitored by immunofluorescence microscopy (Zeiss LSM 710). Cultures with TER values of $\geq$800 Ω/cm^2 and extensive coverage by beating cilia were retained for experimentation.

Bacterial culture and time course infection of WD-NHBE cells. NTHi strain 176, an isolate obtained from the middle ear of a participant in a Finnish otitis media outbreak cohort study, was used in this study (kindly provided by Derek Hood, University Oxford, United Kingdom). The NTHi strain was routinely grown on PoliVitex chocolate agar (bioMérieux) incubated overnight at 37°C with 5% CO_2. For infection studies, NTHi was grown in brain heart infusion (BHI) broth (Difco Laboratories) supplemented with 10 μg/ml each of hemin (Fluka Biochemika) and NAD (Sigma-Aldrich) until the optical density at 600 nm (OD_{600}) reached 0.5 (exponential phase). Bacteria at an OD_{600} of 0.5 were pelleted and resuspended in infection medium comprised of unsupplemented BEBM to prepare the inoculum. WD-NHBE cultures were infected synchronously or were mock infected. All infections (multiplicity of infection, 100 bacteria per cell) were undertaken in triplicate in WD-NHBE cultures after 28 days of growth at the ALI. The inocula or medium-only controls were added to the apical surface of the cultures and incubated for 1 h at 37°C and 5% CO_2. Subsequently, the inoculum was removed, and the apical surface was gently rinsed three times with 500 μl BEBM to remove any nonadherent bacteria. The percentages of cytotoxicity in infected WD-NHBE cells were determined by using an LDH assay cytotoxicity detection kit (Roche Diagnostics, Indianapolis, IN).

For the growth kinetics and survival assay, infection of WD-NHBE was performed as described above. At selected time points, the membranes were thoroughly washed and lysed with 1% saponin (Sigma Aldrich) in infection medium. Total cell-associated bacteria were quantified by counting CFU, and the significance of the results was determined by one-way analysis of variance (ANOVA) followed by the Bonferroni post-test.

Isolation of total RNA from infected cells. Total RNA was isolated at 1, 6, 24, and 72 h from NTHi-infected WD-NHBE cells and corresponding mock controls (three replicates per time point) using TRIzol reagent (Life Technologies). No medium change was performed for time course experiments during RNA extraction in order not to allow any transcriptome bias which might arise due to the addition of fresh medium. Total RNA isolated from bacteria conditioned in infection medium at 37°C in 5% CO_2 for 1 h was used as a bacterial baseline control (t_1c). RNA was treated twice with Turbo DNA-free DNase (Ambion) according to the manufacturer's protocol for rigorous sample treatment. Complete DNA removal was verified by real-time quantitative reverse transcription PCR (qRT-PCR) by amplifying the 16S and glyceraldehyde-3-phosphate dehydrogenase (GAPDH) genes. DNase-treated RNA was purified using the Direct-zol RNA miniprep kit (Zymo) and stored at −80°C until further use. The RNA quality was analyzed using a Bioanalyzer 2100 (Agilent Technologies), and the RNA concentrations were measured using a NanoDrop instrument.

cDNA library construction and Illumina sequencing. cDNA libraries were prepared using reagents and protocols supplied with the ScriptSeq complete gold (epidemiology) low-input kit (Epicentre), using 450 ng of each sample. Briefly, human and bacterial rRNA were depleted using the Ribo-Zero gold (Epidemiology) kit and purified using the ethanol precipitation method. The removal of rRNA was confirmed with the Agilent Bioanalyzer 2100 using the RNA 6000 picokit. Ribodepleted RNA was fragmented chemically, and cDNA was synthesized using random primers (Epicentre). The library was amplified with the unique indexed primers of the ScriptSeq index PCR primer kit (catalog no. RSBC10948; Epicentre) in an amplification protocol of 15 cycles and purified with the AMPure XP purification protocol (Beckman Coulter). The libraries were validated by using high-sensitivity DNA chips on the Agilent Bioanalyzer and quantified by real-time PCR on the 7900 HT fast RT-PCR system (Life Technologies), using the KAPA SYBR fast ABI Prism qPCR kit (Kapa). Sequencing was carried out on the HiSeq 2500 in a 75-bp paired-end run with TruSeq SBS version 3 chemistry (Illumina).

Read mapping and data analysis For the human host transcriptome analysis, reads were aligned in paired-end mode to a human genome (hg19) using the STAR (version 2.3.1n) aligner (45) with the default settings. Mapped data were converted to gene level counts using HTSeq-count and the UCSC annotation (http://genome.ucsc.edu/). Differential expression was evaluated for each time point, comparing the data for the infected sample to the data for the untreated sample using the DESeq Bioconductor package (46). Differential expression was detected using the following thresholds: $|\log_2$-fold change$|$ of $\geq$1 and adjusted P value of $\leq$0.01.

For the bacterial transcriptome analysis, reads were aligned in directional paired-end mode to the Hi176 bacterial genome using the *Rsubread*

Bioconductor package (version 1.14.2) (47). To avoid cross mapping of reads, before any mapping procedure to the bacterial genome, reads from infected samples and t_1c reference samples were aligned to the human genome. Unmapped pairs of reads were then used for the alignment to the bacterial genome. Gene-level counts were computed with the *featureCounts* function of *Rsubread*. Between-sample normalization was applied using the *voom* function of the *limma* Bioconductor package (version 3.20.8) (48). Differential expression was evaluated for each time point, comparing the data for infected samples to the data for t_1c reference samples by linear model fit and eBayes statistics as implemented by the *limma* package (49). Differentially expressed genes were detected using the following thresholds: $|\log_2$-fold change$|$ of ≥ 1 and adjusted P value of ≤ 0.05.

NTHi Hi176 genome assembly and annotation. The genome sequence of the *H. influenzae* strain Hi176 (alias Fi176) was published by De Chiara et al. (50). The genome sequence was assembled using Celera assembler 7 (51) at the level of contigs. The draft genome was annotated using a hybrid approach. The genome annotation was transferred by homology with *RATT* (52). To identify open reading frames (ORFs) in regions that had no close homology to already-annotated strains, we performed a *de novo* ORF prediction using *Glimmer3* (53). The first release of the genome annotation (version 0.1) is available from the Wellcome Trust Sanger Institute ftp site at: ftp://ftp.sanger.ac.uk/pub/project/pathogens/Haemophilus/influenzae/NT_strains/v0.1/Haemophilus_influenzae_Hi176_v0.1.gbk. The published genome was further annotated by comparing predicted genes to clusters of orthologous genes data available from the KEGG database (release 71.0) (54) by FASTA search. Genes were mapped into KEGG metabolic pathways and functional hierarchies. Candidate sRNAs were manually curated by Artemis Genome Browser version 16.0.0 (55) inspection. Putative functions of the candidate sRNAs were identified by BLAST using the Rfam database, available at the Wellcome Trust Sanger Institute (http://rfam.xfam.org/).

Clustering and enrichment analysis. Functional classification of eukaryotic genes was performed using the DAVID online database (56) with Fisher's exact test enrichment statistics and a Benjamini-Hochberg-corrected P value cutoff of 0.05 ($P_{BH} < 0.05$). Ingenuity Pathway Analysis (IPA) software (Ingenuity Systems) was used to discover relevant modulated pathways and transcriptional networks according to Fisher's exact test enrichment statistics and Benjamini-Hochberg-corrected P value calculations. The functional analysis identified the biological functions and/or sets of disease-related genes that were most significantly modulated during the time course. Genes from the data set with more than 2-fold up- or downregulation and a P value of <0.05 that were associated with biological functions and/or sets of disease-related genes in the Ingenuity Knowledge Base were considered for the analysis. The top molecular and cellular functions and top canonical pathways were primarily used in this analysis. Gene expression heat maps were generated using the MultiExperiment Viewer (MEV) software suite (57, 58). Hierarchical clustering was applied using the Euclidean metrics and default parameters. Prokaryotic enrichment analysis was performed by Fisher's exact test and Benjamini-Hochberg correction as implemented by MEV, to test whether a list of differentially regulated genes was particularly rich in genes annotated in a particular KEGG metabolic pathway.

qRT-PCR. For validation of RNA-seq data, 2 μg of DNase I-treated total RNA was reverse transcribed using the GoScript reverse transcription system and random hexamers (Promega, Southampton, United Kingdom). qPCR was performed with a Stratagene Mx3000P qPCR system (Agilent Technologies), using 200 ng cDNA, 0.1 μM gene-specific primers (see Table S3 in the supplemental material), and Power SYBR green master mix (Applied Biosystems). The level of each gene was normalized to that of the housekeeping gene GAPDH, and relative expression shown as the cycle threshold ($2^{-\Delta\Delta CT}$) value. To validate the results obtained in the RNA-seq experiments, qRT-PCR was used to analyze the relative expression levels of 18 genes from different functional categories. The comparison of gene expression by qRT-PCR and RNA-seq analyses showed a significant Pearson correlation between the results of the two approaches ($P < 0.001$, $R = 0.9106$, and $R^2 = 0.8291$) (see Fig. S5A and B in the supplemental material).

To estimate the bacterial RNA concentrations in the mixed transcriptome samples, cDNA was synthesized using 1 μg each of the total RNA of the mixed transcriptome sample (1 hpi) from Hi176-infected NHBE cells at 1 hpi and the artificially mixed transcriptome samples (0, 0.5, 1, 3, 5, 10, and 50% of bacterial RNA) in the SuperScript III first-strand synthesis system (Invitrogen) after DNase I (Turbo; Invitrogen) treatment. The cDNAs were amplified using gene-specific primers designed for the 16S gene. qPCR experiments were performed with three technical replicates in 20-μl reaction mixtures containing 2× SYBR master mix and 1 μl of cDNA template using the Stratagene Mx3005P system. By comparing the C_T values of the mixed transcriptome samples with those of each artificial control sample, the amount of bacterial RNA was estimated to be ~1 to 2% (see Fig. S5C in the supplemental material).

Immunofluorescence microscopy. Mock-infected or NTHi-infected WD-NHBE cultures were rinsed three times with BEBM infection medium, and the epithelium-containing inserts were fixed with 4% paraformaldehyde, except for mucin staining, where a methanol-acetone fixation protocol was used. Membranes were permeabilized and blocked with 3% bovine serum albumin and 0.1% Triton X-100 in phosphate-buffered saline. Incubation with primary antibodies (see Table S3 in the supplemental material) and rabbit anti-total NTHi antiserum was performed either overnight at 4°C or for 2 h at room temperature and followed by treatment with the appropriate Alexa Fluor-conjugated secondary antibody. Samples were mounted using ProLong gold antifade reagent with diamidino-2-phenylindole (DAPI; Invitrogen) and analyzed by confocal microscopy using a Zeiss LSM 710 confocal microscope. z-stack 3-D reconstructions were performed using Imaris software (Bit-Plane, Inc.).

Electron microscopy. For scanning electron microscopy, samples were fixed in 2.5% glutaraldehyde and 2.5% paraformaldehyde in 0.1 M sodium cacodylate buffer overnight, washed in buffer, and secondarily fixed in 1% osmium tetroxide in cacodylate buffer for 1 h. Samples were then washed in water and block stained with 1% uranyl acetate for 1 h. They were dehydrated with ethanol using progressively increasing concentrations and dried by the critical point method using CO_2 in a Balzers Union CPD 020 (BAL-TEC AG), sputter coated with gold in a Balzers MED 010 unit, and observed with a JEOL JSM 6010LA scanning electron microscope. For transmission electron microscopy, samples were fixed and dehydrated as described as above and embedded in Epon-based resin. Ultrathin sections (50 to 70 nm) were cut with a Reichert Ultracut ultramicrotome by using a diamond knife, collected on Formvar copper grids, and stained with uranyl acetate and lead citrate. Observations were made with a JEOL 1200 EXII transmission electron microscope, and micrographs were acquired by the Olympus SIS Veleta charge-coupled device (CCD) camera equipped with iTEM software.

Western blotting. Cells were lysed in radioimmunoprecipitation assay (RIPA) lysis buffer containing 1 mM phenylmethylsulfonyl fluoride (PMSF), 1 mM pepstatin A, 1 mM aprotonin, 1 mM leupeptin, 1 mM NaOrthovanadate, and 1% Triton X-100. Protein concentrations were determined by bicinchoninic acid (BCA) assay (Thermo-Fisher Scientific, Loughborough, United Kingdom). Samples were added to 4× gel loading buffer (Life Technologies), 10× dithiothreitol, and boiled at 100°C for 5 min. Fifteen-microgram amounts of samples were resolved on 4 to 12% bis-Tris gels (Life Technologies), transferred to nitrocellulose membranes, and blocked with 5% milk. Membranes were incubated with antibodies (see Table S3 in the supplemental material) and detected by enhanced chemiluminescence (Thermo Scientific).

Determination of cytokine/chemokine concentrations. To study components of the innate immune responses to NTHi infection, we selected a panel of 40 cytokines/chemokines on the basis of their mRNA levels as detected by RNA-seq. Basolateral medium samples were collected at 6, 24, and 72 hpi in triplicates and were stored at −80°C until use. Samples were then thawed and analyzed for chemokine concentrations

with the Luminex 200 system, using the Bio-Plex pro human chemokine 40-plex panel (Bio-Rad) according to the manufacturer's instructions.

Statistical analysis. Functional assay data are presented as the mean results ± standard errors of the means (SEM). Statistical analyses were performed using GraphPad Prism 5 software (GraphPad Software, Inc.). The unpaired Student's *t* test or one-way ANOVA statistical test, followed by the Tukey or Bonferroni posttest, was applied.

Nucleotide sequence accession number. The RNA sequencing reads have been deposited in the Gene Expression Omnibus (GEO) Sequence Read Archive of the National Center for Biotechnology Information (http://www.ncbi.nlm.nih.gov/geo/) under accession no. GSE63900.

SUPPLEMENTAL MATERIAL

Supplemental material for this article may be found at http://mbio.asm.org/lookup/suppl/doi:10.1128/mBio.01765-15/-/DCSupplemental.

Figure S1, PDF file, 0.8 MB.
Figure S2, PDF file, 0.5 MB.
Figure S3, PDF file, 0.4 MB.
Figure S4, PDF file, 0.4 MB.
Figure S5, PDF file, 0.4 MB.
Table S1, PDF file, 0.1 MB.
Table S2, PDF file, 0.2 MB.
Table S3, PDF file, 0.2 MB.

ACKNOWLEDGMENTS

We thank Nicola Pacchiani for performing data conversion and quality controls of Illumina sequencing, Anja K. Seubert for technical assistance, and Giorgio Corsi for the artwork. We also thank Lorenza Putignani for critical appraisal of metabolic data analysis and Christoph M. Tang, Ennio De Gregorio, and John L. Telford for valuable discussions.

This work was supported by internal funding from GSK vaccines and by the European Community's Seventh Framework Programme EIMID ITN (European Institute of Microbiology and Infectious Diseases Initial Training Network, FP7-PEOPLE-2010-264388). The funder had no role in study design, data collection and interpretation, decision to publish, or preparation of the manuscript.

REFERENCES

1. **Agrawal A, Murphy TF**. 2011. Haemophilus influenzae infections in the H. influenzae type b conjugate vaccine era. J Clin Microbiol **49:** 3728–3732. http://dx.doi.org/10.1128/JCM.05476-11.
2. **Van Schilfgaarde M, van Alphen L, Eijk P, Everts V, Dankert J**. 1995. Paracytosis of Haemophilus influenzae through cell layers of NCI-H292 lung epithelial cells. Infect Immun **63:**4729–4737.
3. **Ren D, Nelson KL, Uchakin PN, Smith AL, Gu X-, Daines DA**. 2012. Characterization of extended co-culture of non-typeable Haemophilus influenzae with primary human respiratory tissues. Exp Biol Med **237:** 540–547. http://dx.doi.org/10.1258/ebm.2012.011377.
4. **St. Geme JW, III, Falkow S**. 1990. Haemophilus influenzae adheres to and enters cultured human epithelial cells. Infect Immun **58:**4036–4044.
5. **Ketterer MR, Shao JQ, Hornick DB, Buscher B, Bandi VK, Apicella MA**. 1999. Infection of primary human bronchial epithelial cells by Haemophilus influenzae: macropinocytosis as a mechanism of airway epithelial cell entry. Infect Immun **67:**4161–4170.
6. **Forsgren J, Samuelson A, Ahlin A, Jonasson J, Rynnel-Dagoo B, Lindberg A**. 1994. Haemophilus influenzae resides and multiplies intracellularly in human adenoid tissue as demonstrated by in situ hybridization and bacterial viability assay. Infect Immun **62:**673–679.
7. **Bandi V, Apicella M, Mason E, Murphy T, Siddiqi A, Atmar R, Greenberg S**. 2001. Nontypeable Haemophilus influenzae in the lower respiratory tract of patients with chronic bronchitis. Am J Respir Crit Care Med **164:**2114–2119. http://dx.doi.org/10.1164/ajrccm.164.11.2104093.
8. **Jenner RG, Young RA**. 2005. Insights into host responses against pathogens from transcriptional profiling. Nat Rev Microbiol **3:**281–294. http://dx.doi.org/10.1038/nrmicro1126.
9. **Rappuoli R**. 2000. Pushing the limits of cellular microbiology: microarrays to study bacteria-host cell intimate contacts. Proc Natl Acad Sci U S A **97:**13467–13469. http://dx.doi.org/10.1073/pnas.010505497.
10. **Ogunniyi AD, Mahdi LK, Trappetti C, Verhoeven N, Mermans D, Van der Hoek MB, Plumptre CD, Paton JC**. 2012. Identification of genes that contribute to the pathogenesis of invasive pneumococcal disease by in vivo transcriptomic analysis. Infect Immun **80:**3268–3278. http://dx.doi.org/10.1128/IAI.00295-12.
11. **De Vries SPW, Eleveld MJ, Hermans PWM, Bootsma HJ**. 2013. Characterization of the molecular interplay between Moraxella catarrhalis and human respiratory tract epithelial cells. PLoS One **8:**e72193. http://dx.doi.org/10.1371/journal.pone.0072193.
12. **Belcher CE, Drenkow J, Kehoe B, Gingeras TR, McNamara N, Lemjabbar H, Basbaum C, Relman DA**. 2000. The transcriptional responses of respiratory epithelial cells to Bordetella pertussis reveal host defensive and pathogen counter-defensive strategies. Proc Natl Acad Sci U S A **97:** 13847–13852. http://dx.doi.org/10.1073/pnas.230262797.
13. **Virtaneva K, Porcella SF, Graham MR, Ireland RM, Johnson CA, Ricklefs SM, Babar I, Parkins LD, Romero RA, Corn GJ, Gardner DJ, Bailey JR, Parnell MJ, Musser JM**. 2005. Longitudinal analysis of the group A streptococcus transcriptome in experimental pharyngitis in cynomolgus macaques. Proc Natl Acad Sci U S A **102:**9014–9019. http://dx.doi.org/10.1073/pnas.0503671102.
14. **Villenave R, Thavagnanam S, Sarlang S, Parker J, Douglas I, Skibinski G, Heaney LG, McKaigue JP, Coyle PV, Shields MD, Power UF**. 2012. In vitro modeling of respiratory syncytial virus infection of pediatric bronchial epithelium, the primary target of infection in vivo. Proc Natl Acad Sci U S A **109:**5040–5045. http://dx.doi.org/10.1073/pnas.1110203109.
15. **Edwards JA, Groathouse NA, Boitano S**. 2005. Bordetella bronchiseptica adherence to cilia is mediated by multiple adhesin factors and blocked by surfactant protein A. Infect Immun **73:**3618–3626. http://dx.doi.org/10.1128/IAI.73.6.3618-3626.2005.
16. **Matrosovich MN, Matrosovich TY, Gray T, Roberts NA, Klenk H-**. 2004. Human and avian influenza viruses target different cell types in cultures of human airway epithelium. Proc Natl Acad Sci U S A **101:** 4620–4624. http://dx.doi.org/10.1073/pnas.0308001101.
17. **Westermann AJ, Gorski SA, Vogel J**. 2012. Dual RNA-seq of pathogen and host. Nat Rev Microbiol **10:**618–630. http://dx.doi.org/10.1038/nrmicro2852.
18. **Huang DW, Sherman BT, Lempicki RA**. 2008. Systematic and integrative analysis of large gene lists using DAVID bioinformatics resources. Nat Protoc **4:**44–57. http://dx.doi.org/10.1038/nprot.2008.211.
19. **Ren D, Kordis AA, Sonenshine DE, Daines DA**. 2014. The ToxAvapA toxin-antitoxin locus contributes to the survival of nontypeable Haemophilus influenzae during infection. PLoS One **9:**e91523. http://dx.doi.org/10.1371/journal.pone.0091523.
20. **Ren D, Walker AN, Daines DA**. 2012. Toxin-antitoxin loci vapBC-1 and vapXD contribute to survival and virulence in nontypeable Haemophilus influenzae. BMC Microbiol **12:**263. http://dx.doi.org/10.1186/1471-2180-12-263.
21. **Norton JP, Mulvey MA**. 2012. Toxin-antitoxin systems are important for niche-specific colonization and stress resistance of uropathogenic Escherichia coli. PLoS Pathog **8:**e1002954. http://dx.doi.org/10.1371/journal.ppat.1002954.
22. **Webb E, Claas K, Downs D**. 1998. thiBPQ encodes an ABC transporter required for transport of thiamine and thiamine pyrophosphate in Salmonella typhimurium. J Biol Chem **273:**8946–8950. http://dx.doi.org/10.1074/jbc.273.15.8946.
23. **Mietzner TA, Tencza SB, Adhikari P, Vaughan KG, Nowalk AJ**. 1998. Fe(III) periplasm-to-cytosol transporters of gram-negative pathogens. Curr Top Microbiol Immunol **225:**113–135. http://dx.doi.org/10.1007/978-3-642-80451-9_7.
24. **Vergauwen B, Elegheert J, Dansercoer A, Devreese B, Savvides SN**. 2010. Glutathione import in Haemophilus influenzae Rd is primed by the periplasmic heme-binding protein HbpA. Proc Natl Acad Sci U S A **107:** 13270–13275. http://dx.doi.org/10.1073/pnas.1005198107.
25. **Whitby PW, Morton DJ, Vanwagoner TM, Seale TW, Cole BK, Mussa HJ, McGhee PA, Bauer CYS, Springer JM, Stull TL**. 2012. Haemophilus influenzae OxyR: characterization of its regulation, regulon and role in fitness. PLoS One **7:**e50588. http://dx.doi.org/10.1371/journal.pone.0050588.
26. **Juneau RA, Pang B, Armbruster CE, Murrah KA, Perez AC, Swords WE**. 2014. Peroxiredoxin/glutaredoxin (pdgX) and catalase (htkE) promote resistance of nontypeable Haemophilus influenzae 86–028NP to oxidant and survival within neutrophil extracellular traps. Infect Immun **83:**239–246. http://dx.doi.org/10.1128/iai.02390-14.
27. **Murphy TF, Brauer AL**. 2011. Expression of urease by Haemophilus

influenzae during human respiratory tract infection and role in survival in an acid environment. BMC Microbiol **11:**183. http://dx.doi.org/10.1186/1471-2180-11-183.

28. **Goodman SD, Obergfell KP, Jurcisek JA, Novotny LA, Downey JS, Ayala EA, Tjokro N, Li B, Justice SS, Bakaletz LO.** 2011. Biofilms can be dispersed by focusing the immune system on a common family of bacterial nucleoid-associated proteins. Mucosal Immunol **4:**625–637. http://dx.doi.org/10.1038/mi.2011.27.
29. **Lu P, Takai K, Weaver VM, Werb Z.** 2011. Extracellular matrix degradation and remodeling in development and disease. Cold Spring Harb Perspect Biol **3:**a005058. http://dx.doi.org/10.1101/cshperspect.a005058.
30. **Demedts IK, Brusselle GG, Bracke KR, Vermaelen KY, Pauwels RA.** 2005. Matrix metalloproteinases in asthma and COPD. Curr Opin Pharmacol **5:**257–263. http://dx.doi.org/10.1016/j.coph.2004.12.005.
31. **Costa C, Rufino R, Traves SL,** Lapa ESJR, Barnes PJ, Donnelly LE. 2008. CXCR3 and CCR5 chemokines in induced sputum from patients with COPD. Chest 133:26–33.
32. **Sharma CM, Darfeuille F, Plantinga TH, Vogel J.** 2007. A small RNA regulates multiple ABC transporter mRNAs by targeting C/A-rich elements inside and upstream of ribosome-binding sites. Genes Dev **21:** 2804–2817. http://dx.doi.org/10.1101/gad.447207.
33. **Santana EA, Harrison A, Zhang X, Baker BD, Kelly BJ, White P, Liu Y, Munson RS, Jr.** 2014. HrrF is the Fur-regulated small RNA in nontypeable Haemophilus influenzae. PLoS One **9:**e105644. http://dx.doi.org/10.1371/journal.pone.0105644.
34. **Juranic Lisnic V, Babic Cac M, Lisnic B, Trsan T, Mefferd A, Das Mukhopadhyay C, Cook CH, Jonjic S, Trgovcich J.** 2013. Dual analysis of the murine cytomegalovirus and host cell transcriptomes reveal new aspects of the virus-host cell interface. PLoS Pathog **9:**e1003611. http://dx.doi.org/10.1371/journal.ppat.1003611.
35. **Humphrys MS, Creasy T, Sun Y, Shetty AC, Chibucos MC, Drabek EF, Fraser CM, Farooq U, Sengamalay N, Ott S, Shou H, Bavoil PM, Mahurkar A, Myers GSA.** 2013. Simultaneous transcriptional profiling of bacteria and their host cells. PLoS One **8:**e80597. http://dx.doi.org/10.1371/journal.pone.0080597.
36. **Bailey KL, LeVan TD, Yanov DA, Pavlik JA, DeVasure JM, Sisson JH, Wyatt TA.** 2012. Non-typeable Haemophilus influenzae decreases cilia beating via protein kinase cepsilon. Respir Res **13:**49. http://dx.doi.org/10.1186/1465-9921-13-49.
37. **He Y, Li H, Zhang J, Hsu C, Lin E, Zhang N, Guo J, Forbush KA, Bevan MJ.** 2004. The extracellular matrix protein mindin is a pattern-recognition molecule for microbial pathogens. Nat Immunol **5:**88–97. http://dx.doi.org/10.1038/ni1021.
38. **Klaile E, Klassert TE, Scheffrahn I, Müller MM, Heinrich A, Heyl KA, Dienemann H, Grünewald C, Bals R, Singer BB, Slevogt H.** 2013. Carcinoembryonic antigen (CEA)-related cell adhesion molecules are co-expressed in the human lung and their expression can be modulated in bronchial epithelial cells by non-typable Haemophilus influenzae, Moraxella catarrhalis, TLR3, and type I and II interferons. Respir Res **14:**85. http://dx.doi.org/10.1186/1465-9921-14-85.
39. **Clarke T, Francella N, Huegel A, Weiser J.** 2011. Invasive bacterial pathogens exploit TLR-mediated downregulation of tight junction components to facilitate translocation across the epithelium. Cell Host Microbe **9:**404–414. http://dx.doi.org/10.1016/j.chom.2011.04.012.
40. **Chu HG, Weeks SK, Gilligan DM, Rockey DD.** 2008. Host alpha-adducin is redistributed and localized to the inclusion membrane in chlamydia- and Chlamydophila-infected cells. Microbiology **154:** 3848–3855. http://dx.doi.org/10.1099/mic.0.2008/020941-0.
41. **Exley RM, Goodwin L, Mowe E, Shaw J, Smith H, Read RC, Tang CM.** 2005. Neisseria meningitidis lactate permease is required for nasopharyngeal colonization. Infect Immun **73:**5762–5766. http://dx.doi.org/10.1128/IAI.73.9.5762-5766.2005.
42. **Exley RM, Wu H, Shaw J, Schneider MC, Smith H, Jerse AE, Tang CM.** 2007. Lactate acquisition promotes successful colonization of the murine genital tract by Neisseria gonorrhoeae. Infect Immun **75:**1318–1324. http://dx.doi.org/10.1128/IAI.01530-06.
43. **Vanderhoeven JP, Bierle CJ, Kapur RP, McAdams RM, Beyer RP, Bammler TK, Farin FM, Bansal A, Spencer M, Deng M, Gravett MG, Rubens CE, Rajagopal L, Adams Waldorf KM.** 2014. Group B streptococcal infection of the choriodecidua induces dysfunction of the cytokeratin network in amniotic epithelium: a pathway to membrane weakening. PLoS Pathog **10:**e1003920. http://dx.doi.org/10.1371/journal.ppat.1003920.
44. **Zhu C, Bai Y, Liu Q, Li D, Hong J, Yang Z, Cui L, Hua X, Yuan C.** 2013. Depolymerization of cytokeratin intermediate filaments facilitates intracellular infection of HeLa cells by Bartonella henselae. J Infect Dis **207:** 1397–1405. http://dx.doi.org/10.1093/infdis/jit040.
45. **Dobin A, Davis CA, Schlesinger F, Drenkow J, Zaleski C, Jha S, Batut P, Chaisson M, Gingeras TR.** 2013. STAR: ultrafast universal RNA-seq aligner. BioInformatics **29:**15–21. http://dx.doi.org/10.1093/bioinformatics/bts635.
46. **Anders S, McCarthy DJ, Chen Y, Okoniewski M, Smyth GK, Huber W, Robinson MD.** 2013. Count-based differential expression analysis of RNA sequencing data using R and Bioconductor. Nat Protoc **8:**1765–1786. http://dx.doi.org/10.1038/nprot.2013.099.
47. **Liao Y, Smyth GK, Shi W.** 2013. The Subread aligner: fast, accurate and scalable read mapping by seed-and-vote. Nucleic Acids Res **41:**e108. http://dx.doi.org/10.1093/nar/gkt214.
48. **Ritchie ME, Phipson B, Wu D, Hu Y, Law CW, Shi W, Smyth GK.** 2015. Limma powers differential expression analyses for RNA-sequencing and microarray studies. Nucleic Acids Res **43:** http://dx.doi.org/10.1093/nar/gkv007.
49. **Smyth GK.** 2004. Linear models and empirical Bayes methods for assessing differential expression in microarray experiments. Stat Appl Genet Mol Biol **3:**1–25. http://dx.doi.org/10.2202/1544-6115.1027.
50. **De Chiara M, Hood D, Muzzi A, Pickard DJ, Perkins T, Pizza M, Dougan G, Rappuoli R, Moxon ER, Soriani M, Donati C.** 2014. Genome sequencing of disease and carriage isolates of nontypeable Haemophilus influenzae identifies discrete population structure. Proc Natl Acad Sci U S A **111:**5439–5444. http://dx.doi.org/10.1073/pnas.1403353111.
51. **Myers EW, Sutton GG, Delcher AL, Dew IM, Fasulo DP, Flanigan MJ, Kravitz SA, Mobarry CM, Reinert KH, Remington KA, Anson EL, Bolanos RA, Chou HH, Jordan CM, Halpern AL, Lonardi S, Beasley EM, Brandon RC, Chen L, Dunn PJ, Lai Z, Liang Y, Nusskern DR, Zhan M, Zhang Q, Zheng X, Rubin GM, Adams MD, Venter JC.** 2000. A whole-genome assembly of drosophila. Science **287:**2196–2204. http://dx.doi.org/10.1126/science.287.5461.2196.
52. **Otto TD, Dillon GP, Degrave WS, Berriman M.** 2011. RATT: Rapid Annotation Transfer Tool. Nucleic Acids Res **39:**e57. http://dx.doi.org/10.1093/nar/gkq1268.
53. **Delcher AL, Bratke KA, Powers EC, Salzberg SL.** 2007. Identifying bacterial genes and endosymbiont DNA with Glimmer. Bioinformatics **23:**673–679. http://dx.doi.org/10.1093/bioinformatics/btm009.
54. **Kanehisa M, Goto S, Sato Y, Kawashima M, Furumichi M, Tanabe M.** 2014. Data, information, knowledge and principle: back to metabolism in KEGG. Nucleic Acids Res **42:**D199–D205. http://dx.doi.org/10.1093/nar/gkt1076.
55. **Rutherford K, Parkhill J, Crook J, Horsnell T, Rice P, Rajandream M-, Barrell B.** 2000. Artemis: sequence visualization and annotation. Bioinformatics **16:**944–945. http://dx.doi.org/10.1093/bioinformatics/16.10.944.
56. **Huang DW, Sherman BT, Lempicki RA.** 2009. Bioinformatics enrichment tools: paths toward the comprehensive functional analysis of large gene lists. Nucleic Acids Res **37:**1–13. http://dx.doi.org/10.1093/nar/gkn923.
57. **Saeed AI, Bhagabati NK, Braisted JC, Liang W, Sharov V, Howe EA, Li J, Thiagarajan M, White JA, Quackenbush J.** 2006. TM4 microarray software suite. Methods Enzymol **411:**134–193. http://dx.doi.org/10.1016/S0076-6879(06)11009-5.
58. **Saeed AI, Sharov V, White J, Li J, Liang W, Bhagabati N, Braisted J, Klapa M, Currier T, Thiagarajan M, Sturn A, Snuffin M, Rezantsev A, Popov D, Ryltsov A, Kostukovich E, Borisovsky I, Liu Z, Vinsavich A, Trush V, Quackenbush J.** 2003. TM4: a free, open-source system for microarray data management and analysis. Biotechniques **34:**374–378.